ISIJ International, Vol. 54 (2014), No. 3, pp. 482–488

Coil Design in Electromagnetic Induction-controlled Automated Steel-teeming System and Its Effects on System Reliability

Xing'an LIU, Qiang WANG,* Dejun LI, Guanlin LI, Dianqiao GENG, Ao GAO and Jicheng HE

Key Laboratory of Electromagnetic Processing of Materials (Ministry of Education), Northeastern University, Shenyang, 110819 China.

(*Received on August 29, 2013; accepted on January 7, 2014*)

To guide the application of a new automated steel-teeming system which in continuous casting is controlled by electromagnetic induction technology, the parameters of the induction coil and system reliability need to be analyzed. The teeming time of an industrial ladle (1.5 t) with the new system was investigated using experimental and numerical methods. The calculated results were consistent with experimental data. The dependence of teeming efficiency on coil parameters for a larger ladle (300 t) was investigated; the influence of the electromagnetic induction system on the temperature and equivalent stress distribution in the ladle system was also analyzed. The results provided optimum coil parameters for a larger ladle normally used in continuous casting processing. An installed coil with surrounding insulating material had little influence on temperature distribution, thermal stability, and structural safety of the ladle. The ladle lining and insulation met safety requirements established for the system. The coil and the steel shell performed reliably during induction heating of steel while teeming. Therefore, the electromagnetic induction-controlled automated steel-teeming system can be safely used in steel production.

KEY WORDS: electromagnetic metallurgy; continuous casting; steel-teeming; reliability; induction heating.

1. Introduction

The ladle-teeming system plays an important role ensuring normal operations in the continuous casting of steel.[1–3] The slide gate nozzle is still the main apparatus of a conventional ladle-teeming method.[4–7] The free opening rate of this method is only about 98% and the nozzle sand filling the upper nozzle can contaminate the molten steel.[8–12] Aimed at resolving these problems, a new method [an electromagnetic induction-controlled automated steel-teeming (EICAST) method] was proposed by Qiang Wang[13–15] *et al*. The basic idea of the method is using an induction coil located in the nozzle brick to melt part or all of the new well-packing material (*i.e*., Fe–C alloy with a similar composition of molten steel), which replaces the conventional nozzle sand, and to achieve smooth automated steel teeming. The new method can achieve a 100% free opening rate and overcome contamination from nozzle sand.[16,17]

In the early stage of our research, the laboratory experiments were done using in-house-designed devices (20 kg) with this new method.[17–20] With these devices, coil and electric current parameters were assessed using numerical simulation methods.[16,17,21] Preliminary work was done based on small prototypes of the devices in the laboratory to verified the feasibility of the technique and provide a theoretical basis in understanding the system. However, the working conditions of the large ladle used in production are complicated, so it was necessary to further study the dependence of teeming efficiency on coil parameters through industrial experiments. On the one hand, the working conditions of the coil should be investigated by such experiments to ensure coil design is correct for the demands of the task. On the other hand, there are practical gains in studying coil parameters to improve heating efficiency of the coil and shorten teeming times of the ladle. Because the large ladle normally used in production needs to operate stably, the designed system should be practical and reliable. Implementing the new system would influence the temperature and stress distribution of the ladle; hence the thermal stability and structural safety of the ladle might be affected. Thus system reliability needs to be analyzed.

Industrial experiments were conducted using an industrial ladle (1.5 t) with the EICAST system and numerical simulations of the experimental process were performed. Based on both studies, coil parameter effects on teeming efficiency of the ladle (300 t) were assessed. The implementation of the coil, the insulating layer, and the Fe–C alloy were analyzed from the perspective of ladle safety. Finally, with the coil operating correctly, system reliability was evaluated. All these aspects are discussed below.

This article is one which was originally scheduled for publication in the special issue (Vol. 54, No. 2) on "Cutting Edge of Computer Simulation of Solidification, Casting and Refining" and instead was specially published in this regular issue.

* Corresponding author: E-mail: wangq@mail.neu.edu.cn

DOI: http://dx.doi.org/10.2355/isijinternational.54.482

2. Experimental Method

To investigate coil temperature, the effect of coil structure on teeming efficiency for the new system was analyzed; the correctness of the model was also verified. Industrial experiments were conducted on the industrial ladle (1.5 t) with the EICAST system in a steel plant. A schematic diagram of the experimental apparatus is presented in **Fig. 1**. In the new system, the ladle bottom and the nozzle brick were modified as follows: the ladle bottom shell was reamed (centered around the nozzle, radius 110 mm); the nozzle brick was hollowed out (height 270 mm, radius 95 mm) to receive the coil and the insulating layer; the insulating layer (zirconia fiber, thickness 10 mm) and the coil (height 102 mm, radius 70 mm, side length of square brass 10 mm, sidewall thickness 2 mm, vertical distance from steel surface to top of coil 90 mm) were placed in hollowed nozzle brick; WRN-type thermocouples (nickel chromium-nickel silicon) were arranged at the top (point a) and bottom (point b) of the coil to monitor the temperature of the coil and the nozzle brick; free space was filled and pounded with fine sand (chromium corundum of a similar composition to the nozzle brick); the gap in the ladle shell formed during reaming was packed tightly with a thickened non-magnetic steel plate. The packed ladle was examined for proper securing, then the ladle was transported to the preparation workshop and baked at 773 K for 72 hours.

The thermocouples were switched on at the beginning of the experiments. The ladle was preheated using a high-temperature flame (1 173 K) for four hours. Molten steel (1 873 K, 1.2 t) was poured into the ladle after the ladle reached its thermal saturation, and a thermocouple of type WRN5T-135 was inserted into the center of the molten steel to measure temperatures. The coil was connected to the induction power supply with quick plugs after the ladle was transported to the teeming position, then the sliding plate was opened to begin steel teeming. After the grains of the Fe–C alloy that had not sintered had freely settled under gravity, the power supply was turned on to heat the sintered Fe–C alloy until the alloy melted. During this period, power supply parameters and teeming time were recorded.

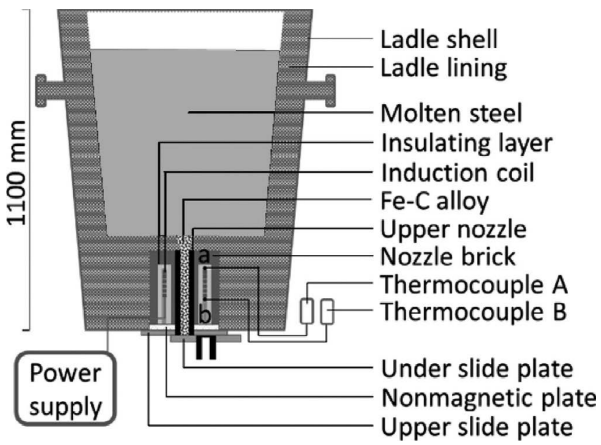

Fig. 1. Schematic diagram of ladle (1.5 t) with the EICAST system.

3. Numerical Simulations

3.1. Modeling

Finite element analysis models were generated of the prototype ladle (1.5 t) and the large production ladle (300 t) as reference objects [see **Figs. 2**(a) and 2(b)]. Because of the relatively small size of the nozzle brick, its placement had little influence on the temperature distribution within the ladle. Therefore the ladle model was simplified to a two-dimensional axial-symmetric shape. The semi-cross sections of both ladles are the research objects. Fine meshing was used for the nozzle brick and the coil to investigate in detail the working temperature of the coil.

3.2. Basic Assumptions

Because of the complexity of the EICAST system, the assumptions made are as follows:

(1) the current density through the inner cross-section of coil is uniform.

(2) the materials comprising the ladle shell and lining are

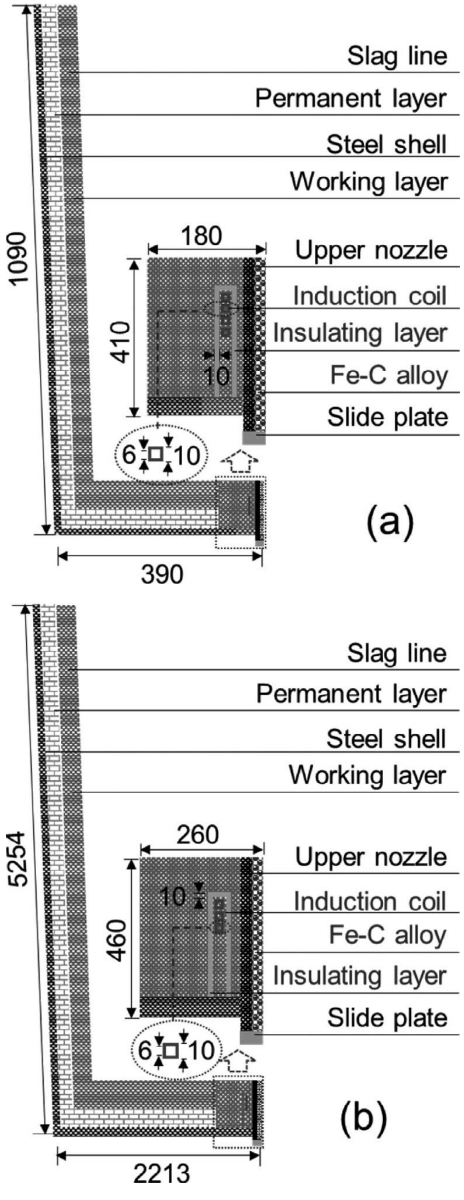

Fig. 2. Simulation models of the ladles with the EICAST system (unit: mm): (a) 1.5-t ladle and (b) 300-t ladle.

Table 1. Physical parameters of ladle materials.[16)]

	Working layer	Permanent layer	Slag line	Nozzle brick	Upper nozzle	Steel shell
Density, kg/m^3	2 950	2 800	290	3 040	350	7 830
Specific heat, kJ/(kg·K)	1 150	956	1 080	1 130	812	550
Thermal conductivity, W/(m·k)	1.15	2.1	10.5	2.2	5.6	24
Thermal expansion coefficient						1.3e-5
Elastic modulus, Mpa	900	850	18 300	1 420	14 500	202 000
Poisson ratio	0.21	0.21	0.22	0.22	0.22	0.3

isotropic; lining thickness is constant (corrosion of the lining is neglected).

(3) the Fe–C alloy is well packed in the nozzle (gaps among the Fe–C alloy particles are ignored).

(4) heat convection in the molten steel is neglected to simplify the calculation when the ladle is standing. The temperature of the molten steel is 1 873 K.

(5) the ladle is in contact with air; the heat transfer coefficient is equal to 10.2 W/(m^2·K) with an initial air temperature of 303 K.

For calculations, the physical parameters of the ladle are taken from the **Table 1**; the thermal conductivity and enthalpy for Fe–C alloy which change with temperature, are given in Refs. 22–24).

3.3. Theoretical Foundations

The procedure employed in the highly coupled magnetic-thermal-structural calculations involved in the analysis of EICAST processes is as follows: the Joule heat generated by inductive current is obtained by solving electromagnetic field; with the Joule heat as a source, the temperature and the stress distributions are obtained. For the theoretical foundations underpinning the magnetic-thermal coupling calculation, see Ref. 16).

For an elastic body, strain depends on temperature and consists of two contributions: one due to the temperature change and the other caused by mechanical stress. For an isotropic material, only linear strains occur under thermal expansion and the shear strain vanishes. Hence the strain component for an elastic body caused by temperature change can be written:

$$\begin{cases} \varepsilon_x = \varepsilon_y = a(\Delta T) \\ \gamma_{xy} = 0 \end{cases} \quad \text{..... (1)}$$

where ε_x, ε_y, are the positive strains; γ_{xy}, shear strain; a, linear expansion coefficient; and ΔT, temperature change (K).

The total strain for an elastic body can be given as:

$$\begin{cases} \varepsilon_x = \dfrac{1}{E}\left[\sigma_x - \mu\sigma_y\right] + a(\Delta T) \\ \varepsilon_y = \dfrac{1}{E}\left[\sigma_y - \mu\sigma_x\right] + a(\Delta T) \\ \gamma_{xy} = \dfrac{2(1+\mu)}{E}\tau_{xy} \end{cases} \quad \text{..... (2)}$$

where σ_x, σ_y, are positive stress (MPa); E, elastic modulus (MPa); τ_{xy}, shear stress (MPa); and μ, Poisson's ratio.

Let ε_0 denote $a(\Delta T)$; the relationship between stress and strain obeys the Hooke Law in the scope of material elasticity and it can be described as:

$$\sigma = D(\varepsilon - \varepsilon_0) \quad \text{..... (3)}$$

where D, is the elastic matrix taking the form:

$$D = \frac{E}{1-\mu^2}\begin{bmatrix} 1 & \mu & 0 \\ \mu & 1 & 0 \\ 0 & 0 & \dfrac{1-\mu}{2} \end{bmatrix} \quad \text{..... (4)}$$

In addition, the relationship between strain and displacement can be expressed as:

$$\begin{cases} \varepsilon_x = \dfrac{\partial u}{\partial x} \\ \varepsilon_y = \dfrac{\partial v}{\partial y} \\ \gamma_{xy} = \dfrac{\partial u}{\partial x} + \dfrac{\partial v}{\partial y} \end{cases} \quad \text{..... (5)}$$

In the solving procedure, the thermal displacement of each node is calculated, followed by the strain for each node. Finally, the stress is found based on the relationship between strain and stress.

4. Results and Discussion

4.1. Comparison between the Calculated and Experimental Results

To verify the accuracy of the model, the pilot-scale tests were done on the industrial ladle (1.5 t) with different power-supply values (20, 25, 30, 35 kW) at a frequency of 15.2 kHz. The teeming times were recorded. From the parameter settings for each experiment, teeming times were also calculated. From the resultant plots (see **Fig. 3**) experimental times are found to be larger than the calculated times. This is because wires are used to connect the power supply with the coil in the experiments. During the heating process, Joule heat was generated when the current flowed through the wires. This could cause energy losses. In addition, the electronic components used in power supply could also cause energy losses. However, the change trend of the calculated values was consistent with the experiment results. Because of the similar structure, materials, and technological process of the experimental ladle (1.5 t) and the large ladle (300 t), as well as the similar size of the coils fitted for the two ladles, this finite element model can be used to predict process parameters for the large ladle (300 t) fitted with the EICAST system.

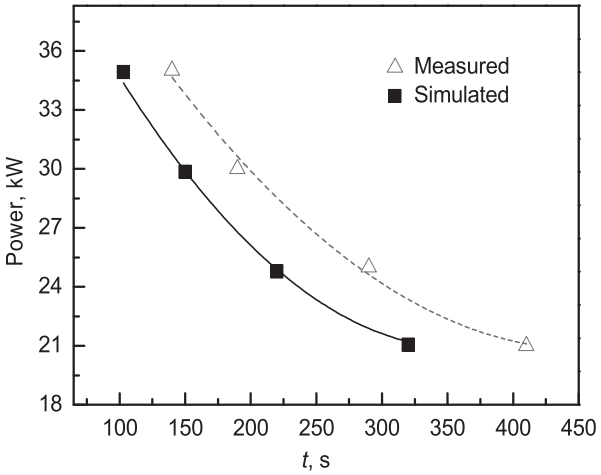

Fig. 3. Simulated and measured teeming times for the 1.5-t ladle under different power-supply setting.

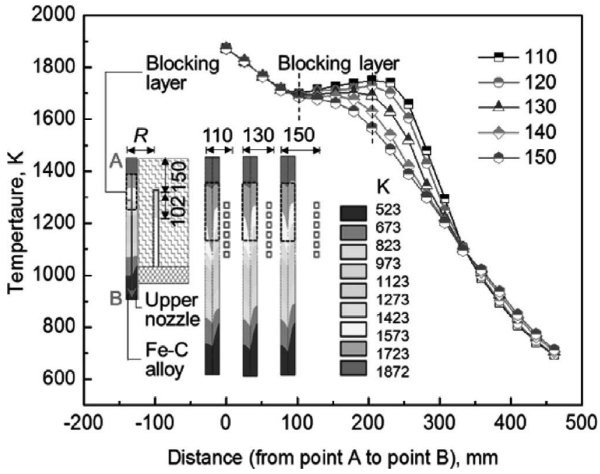

Fig. 4. Temperature distributions (bottom-left corner) and surface temperature profile (top-right corner) for the Fe–C alloy with different *R*.

4.2. Effect of Coil Parameters on Heating Efficiency

Ladle teeming times in continuous casting production should be short. Power-supply settings and coil structure parameters strongly influence heating efficiency given the same physical parameters for the Fe–C alloy.[16] Coil position and structure parameters cannot be changed after the system is packaged although the power settings (current, voltage, frequency, and phase) can be adjusted; the settings used in the calculations are: frequency 15.2 kHz; power, 35 kW. Thus the effects of coil parameters (radius *R*, length *L*, distance *P* between molten steel and coil) on teeming efficiency need to be investigated in detail at the design stage.

Because of the effects of the molten steel and the temperature gradient distribution, the Fe–C alloy filling the upper nozzle separate into five layers. From top to bottom these layers are labeled: melted, solidified, liquid-sintered, solid-sintered, and original.[18] Because of the presence of the solidified, liquid-sintered, and solid-sintered layers, which constituted the blocking function of traditional nozzle sand, molten steel could not flow through upper nozzle. Here, the three layers will be called the blocking layer. Previous studies[18] showed that the thickness of the blocking layer was constant when the molten steel was at a fixed temperature and the temperature range of the blocking layer was from 1 323 K to 1 732 K. Therefore, for our study, it is supposed that, if the temperature of the Fe–C alloy is below 1 323 K, the Fe–C alloy is in its original state and can flow down freely after opening the nozzle; if the surface temperature of the blocking layer is above 1 732 K, the blocking layer can be melted, thereby initiating electromagnetic steel-teeming.

The heating efficiency of the system, in our study, means the melting degree of the blocking layer of the Fe–C alloy while the system has been operated for two minutes. The melting degree of the blocking layer depends on the temperature of the blocking layer. Through analyzing the temperature changes of the blocking layer of the Fe–C alloy, the melting degree of the blocking layer can be investigated. Thus the heating efficiency of the system can be investigated by analyzing the temperature of the blocking layer of the Fe–C alloy.

4.2.1. Effect of Coil Structure

In accordance with the principle of induction heating, an alternating magnetic field which induces electrical currents in the Fe–C alloy was generated around the coil during the heating process. One part of the field is absorbed by the Fe–C alloy and produces Joule heat; another part of the field, which passes through the space between alloy and coil, produces flux leakage that cause energy losses. Hence, to increase the heating efficiency of the system and reduce the teeming time, this clearance space should be kept as small as possible. However, because of the high temperature within the nozzle, the narrow space would increase the coil working temperature. Thus it would decrease heating efficiency and coil safety. Therefore, to select an optimum *R*, coil working temperature and heating efficiency require comprehensive analysis.

Figure 4 shows the temperature distributions (bottom-left corner) and the surface temperature profile (top-right corner) for the Fe–C alloy at different *R* under the conditions (*L*, 102 mm; *P*, 150 mm; power, 35 kW). With decreasing *R*, Fig. 4 indicates that the gap between coil and alloy decreases and hence the heating efficiency of the system clearly increases. When $R \geq 130$ mm, the lowest surface temperature for the blocking layer is below 1 732 K; recall that the role of this layer is to prevent molten steel flowing into the upper nozzle. This means that the blocking layer cannot melt. With $R = 110$ mm and $R = 120$ mm, the lowest surface temperature of the blocking layer is above 1 732 K and the blocking layer melts smoothly. However, too small an *R* reduces the distance between coil and the high-temperature nozzle, thereby increases the working temperature and decreases heating efficiency and coil safety. For a reduced coil working temperature, increased coil safety, and suitable space clearance, the optimal *R* is 120 mm.

The coil length *L* can make a significant impact on the system heating efficiency.[16] **Figure 5** shows the lowest surface temperature profile of the blocking layer and the highest temperature profile of the coil for different *L* under the conditions (*R*, 120 mm; *P*, 150 mm; power, 35 kW). From Fig. 5, with increasing *L*, the central area of the induction heating, with the highest heating efficiency, increases. When

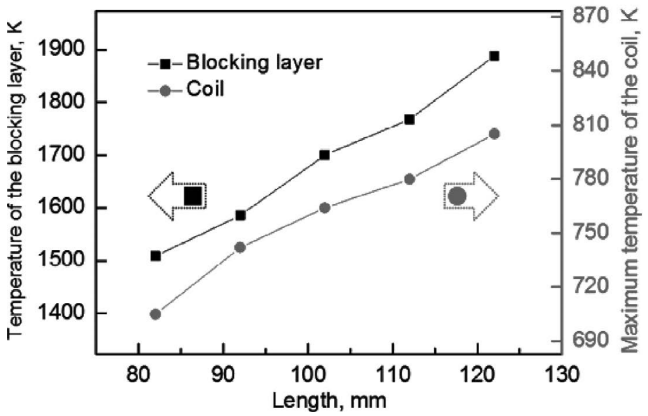

Fig. 5. Lowest surface temperature profile for the blocking layer and highest temperature profile for the coil at different *L*.

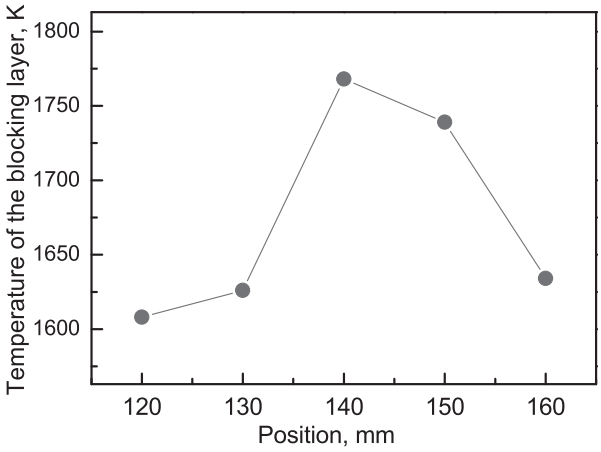

Fig. 6. Lowest surface temperature profile of the blocking layer with different *P*.

$L \leq 92$ mm, the lowest surface temperature of the blocking layer is below 1 732 K. When L is 102 mm, 112 mm, and 122 mm, the lowest surface temperature of the blocking layer is above 1 732 K and the highest temperature of the coil is 764 K, 780 K, and 805 K, respectively. To reduce the working temperature, meet space clearance levels, and enhance the safety of the coil, L = 102 mm is the optimal length.

4.2.2. Effect of Coil Position

The thickness of the blocking layer is about 90 mm.[18] To shorten teeming times the blocking layer should be made entirely within the central heating area of the coil where the heating efficiency is maximal. **Figure 6** shows the lowest surface temperature profile of the blocking layer with different P under the settings (R, 120 mm; L, 102 mm; power, 35 kW). From Fig. 6, the coil heating efficiency clearly changes with P. If $P \leq 130$ mm or $P \geq 160$ mm, the blocking layer is not entirely in the central area and this reduces the heating efficiency. With P = 140 mm and P = 150 mm, the blocking layer temperature has increased. However, as P increases, the coil temperature increases. Therefore, to reduce the working temperature, to increase the heating efficiency, and to ensure coil safety, P = 150 mm is the best position setting.

To sum up, the optimal coil settings appropriate for the large ladle (300 t) found in this study are R = 120 mm, L = 102 mm, and P = 150 mm.

4.3. Effect of Optimal Coil Settings on System Reliability

When the ladle achieves thermal saturation, it also reaches its highest temperature. Because thermal stability and ladle safety are inversely proportional to the ladle temperature, these two response parameters are the poorest when thermal saturation is reached. To ensure normal use from the coil operating in complex and poor working conditions, ladle reliability was evaluated at thermal saturation.

4.3.1. Analysis of The System Reliability When the Coil Does Not Work

The ladle temperature distribution determines its thermal stability during operations, and hence operation safety. Because of the characteristics of the EICAST system, the coil should be installed in the nozzle brick to heat the Fe–C alloy. To analyze the effect of the implementation of the designed coil on thermal stability, the temperature distributions of a traditional ladle and the new ladle with the EICAST system were computed (see **Fig. 7**) when the ladles were at thermal saturation.. These distributions show that because of alloy sizes, the coil and the heat insulating layers are relatively small. The system then has little influence on the temperature distribution of the sidewall and the bottom (except for the nozzle brick) of the ladle. Thus, these two types of ladles have for the most part the same thermal stability. Because of the advantage in thermal conductivity of the Fe–C alloys over nozzle sand, the heat from the nozzle brick in the ladle with the new system conducts downward smoothly. Thus only changes in the temperature gradient of the nozzle brick result; the temperature of the nozzle brick does not increase, and hence has little impact on the thermal stability of the nozzle. However, installing of the heat insulating layer prevents heat transfer and increases this thermal stability. Moreover, the heat insulating layer can effectively reduce the coil working temperature and enable the coil to operate normally under high temperatures in the nozzle brick. As a consequence, compared with the traditional ladle, the implementation of the system has little influence on the ladle temperature distribution as the two types of ladles have a similar temperature distribution. Thermal stability is also similar for both.

Changes in ladle temperature cause expansions or contractions of the ladle shell and linings. These differences in particular produce stress in the lining. Although the new system can meet thermal stability requirements set for the ladle and has little influence on its temperature distribution, slight changes can impact on the stress distribution produce stress points. These stress points can cause damage to the ladle and directly impact on ladle longevity and safety. Therefore a stress analysis of the ladle with the new system is needed to ensure the ladle operates within applied safely limits.

The equivalent stress distributions of the two types of ladles (see **Fig. 8**) show that the maximum equivalent stresses of the working lining, the permanent lining, and the nozzle brick of the ladle with the new system are similar to those for the traditional ladle; these values are 33 MPa, 20

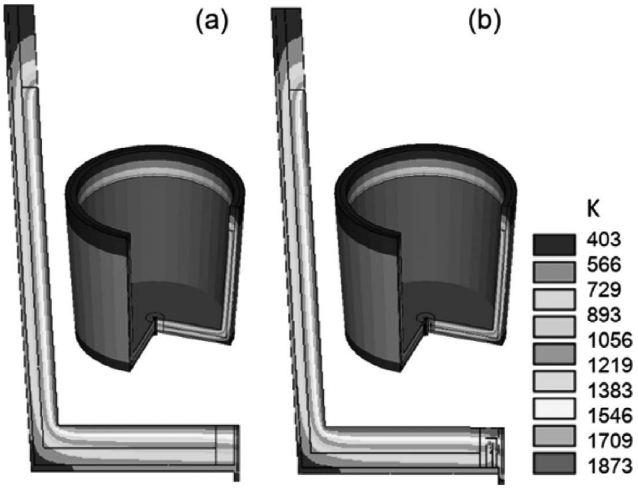

Fig. 7. Temperature distributions for the two types of ladles: (a) the traditional ladle and (b) the ladle with the EICAST system.

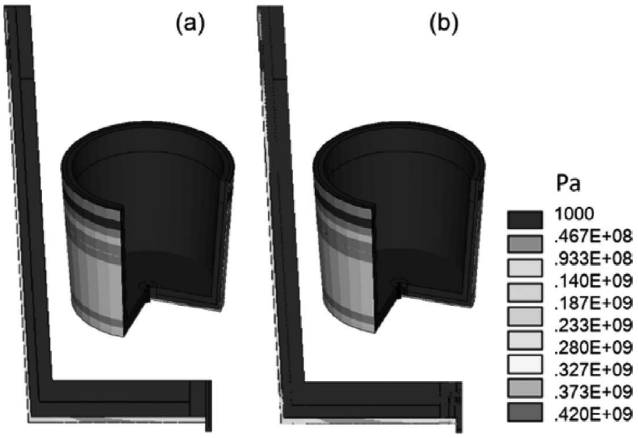

Fig. 8. Equivalent stress distributions for the two types of ladles: (a) the traditional ladle and (b) the new ladle with the EICAST system.

MPa, and 27.6 MPa respectively. The values are all within safe limits. The maximum equivalent stresses for the installed coil is 54 MPa, less than its compressive strength at high temperature, 102 MPa; the maximum equivalent stress of the heat insulating layer is 38.1 MPa, less than its compressive strength of 87 MPa at high temperature. These values are also within safe limit. Moreover, these stress distributions are similar for both ladle types, a consequence of the fact that changes in the ladle with the new system are only slight. With similar temperature distributions, thermal stresses, which play a leading role in the ladle stress when the ladles are at thermal saturation, are also similar. Hence, they have similar structure safety levels and can be used in continuous casting production in safety.

4.3.2. Analysis of the System Reliability When the Coil Works

From the characteristics of the EICAST system, the coil needs cooling when the coil works. At this instant, the temperature of the nozzle brick is lower than that when the coil does not work. (From Fig. 1, for the 1.5-t ladle, the experimentally measured temperature of point a is 766 K when the coil is with cooling; the temperature of the point a is 611 K

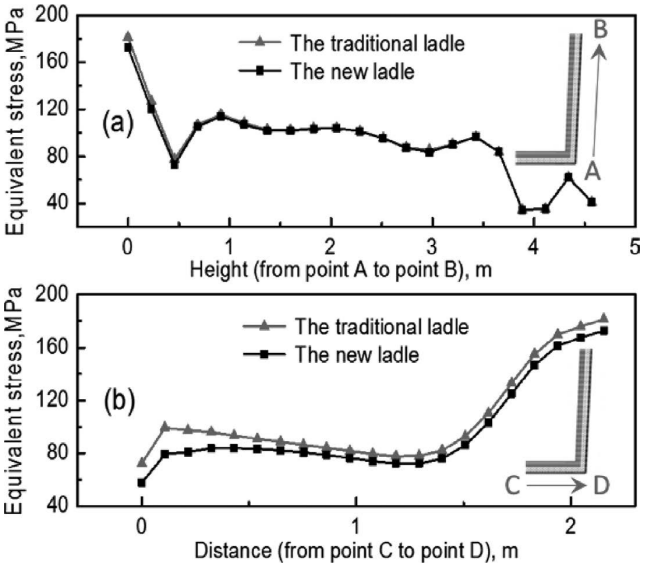

Fig. 9. Equivalent stress profiles of the traditional ladle and the new ladle with the EICAST system: (a) the lateral shell and (b) the bottom shell.

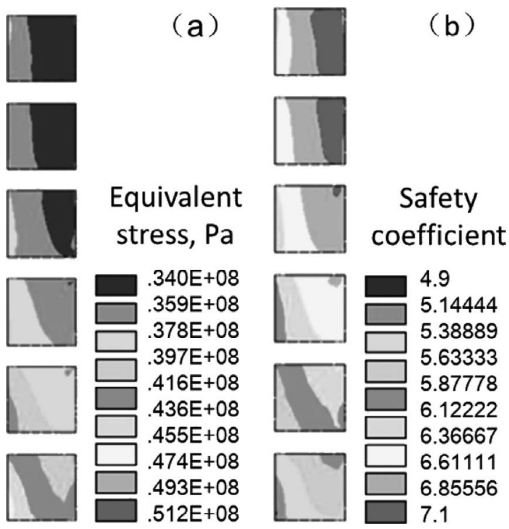

Fig. 10. Equivalent stress distribution (a) and safety factor distribution (b) for the working coil.

when the coil is without cooling). Because induction heating has little influence on nonmagnetic substances, there is no influence on the thermal stability and reliability of the ladle's nonmagnetic parts (ladle lining, nozzle brick, nozzle, insulting layer) when the coil is operating. For the other parts, such as the ladle shell and the coil, the safety of these parts could be reduced because of the self-heating of the coil and the effect of induction heating on the ladle shell during heating. To ensure good system reliability, further analysis is required as the coil operates.

The equivalent stress profiles for both ladles (see **Fig. 9**) show that the stress along the lateral wall of the ladle with the new system is similar to the traditional ladle. Both would then have the same level of safety. With the presence of the insulting layer and the cooling of the coil, temperatures are reduced in the nozzle brick and the ladle's bottom shell. This can cause decreases in thermal stress and equivalent stress of the new ladle with the EICAST system. Thus we con-

clude that the ladle shell operates with a high level of safety when the coil is working.

The equivalent stress and the safety factor (the ratio of equivalent stress to yield strength) charts for the working coil (see **Fig. 10**) indicate that, with the cooling of the coil, the maximum equivalent stress of the coil is 49.2 MPa, which is less than the 54 MPa when the coil was not working. Concurrently, given yield strength for copper of 170 MPa–250 MPa, the coil can be used normally. The safety factor chart of the working coil (Fig. 10(b)) suggests that the minimum safety factor is about 4.9, which meets the safety requirements set for the coil. Therefore, regardless of whether the coil works, the coil used in the EICAST system has a high level of reliability and can be safely operated in continuous casting production.

5. Conclusions

(1) Industrial experiments and numerical simulations were employed to investigate the teeming time of an industrial ladle (1.5 t) with the EICAST system. The calculated results were consistent with experimental data and the correctness of the model was verified.

(2) The effect of varying coil parameters on heating was quantitatively studied. The optimal coil settings suitable for a 300-t ladle with the EICAST system were found to be: R = 120 mm, L = 102 mm, P = 150 mm.

(3) When the coil is not functioning, the temperature and the equivalent stress distribution of the ladle using the new system are similar to those for the traditional ladle, and all components of the ladle meet requirement levels for thermal stability and structure safety; when the coil is functioning, the maximum equivalent stress and the minimum safety factor of the coil are 49.2 MPa and 4.9, respectively, with the steel shell and the coil both meeting the safety requirement levels. Therefore, the EICAST system can be used in continuous casting production safely.

Acknowledgments

This study is financially supported by the "111 project" (B07015) and the Open Foundation of State Key Laboratory of Advanced Metallurgy of University of Science and Technology Beijing.

REFERENCES

1) G. M. Mazzaferro, M. Piva, S. P. Ferro, P. Bissio, M. Iglesias, A. Calvo and M. B. Goldschmit: *Ironmaking Steelmaking*, **31** (2004), 503.
2) C. Gheorghies, I. Crudu, C. Teletin and C. Spanu: *J. Iron Steel Res. Int.*, **16** (2009), 12.
3) L. T. Wang, C. H. Deng, M. Dong, L. F. Shi and J. P. Zhang: *J. Iron Steel Res. Int.*, **19** (2012), 1.
4) V. A. Kononov, N. V. Kononov and V. P. Vasilenko: *Refract. Ind. Ceram.*, **52** (2011), 118.
5) N. Kubo, J. Kubota and T. Ishii: *ISIJ Int.*, **41** (2001), 1221.
6) N. P. Solomin and V. I. Zolotukhin: *Metallurgist*, **41** (1997), 89.
7) K. K. Kappmeye and J. T. Shapland: *J. Iron Steel Inst.*, **210** (1972), 751.
8) International Iron and Steel Institute: IISI Study on Clean Steel, Metallurgial Industry Press, Bejing, (2006), 4.
9) F. P. Pleschiutschnigg, L. Parschat, W. Rahmfeld and H. F. Schrewe: *Iron Steel Eng*., **64** (1987), 51.
10) H. Tanaka, R. Nishihara, I. Kitagawa and R. Tsujino: *ISIJ Int.*, **33** (1993), 1238.
11) H. Tanaka, R. Nishihara, R. Miura, R. Tsujino, T. Kimura, T. Nishi and T. Imoto: *ISIJ Int.*, **34** (1994), 868.
12) I. G. Voronin, V. A. Bezgodov, S. K. Fliatov, Yu. I. Pyatinin, V. A. Savchits and K. I. Kuznetsov: *Metallurgist*, **5** (1983), 22.
13) Q. Wang, D. J. Li, X. A. Liu, H. S. Chai, K. Marukawa and J. C. He: China Pat, 201110220532.2, (2011).
14) J. C. He, K. Marukawa and Q. Wang: China Pat, ZL1810417, (2006).
15) A. Gao, Q. Wang, C. J. Wang, K. Wang and J. C. He: China Pat, CN 101537476a, (2009).
16) A. Gao, D. J. Li, Q. Wang, K. Wang, B. G. Jin, K. Marukawa and J. C. He: *ISIJ Int.*, **50** (2010), 1770.
17) A. Gao, Q. Wang, D. J. Li, B. G. Jin, K. Wang and J. C. He: *Acta Metall. Sin. (China)*, **46** (2010), 634.
18) A. Gao, Q. Wang, D. J. Li, H. S. Chai, L. J. Zhao and J. C. He: *Acta Metall. Sin*. (*China*), **47** (2011), 219.
19) D. J. Li, X. A. Liu, Q. Wang, R. H. Ouyang, H. S. Chai and J. C. He: *J. Iron Steel Res. Int.*, **24** (2012), 16.
20) D. J. Li, X. A. Liu, Q. Wang and J. C. He: *J. Northeastern Univ. (Nat. Sci.*), **33** (2012), 661.
21) A. Gao, Q. Wang, B. G. Jin and J. C. He: *J. Northeastern Univ. (Nat. Sci.*), **31** (2010), 515.
22) K. Sadeghipour, J. A. Dopkin and K. Li: *Comput. Ind*., **28** (1996), 195.
23) J. Y. Jang and Y. W. Chiu: *Appl. Therm. Eng.*, **27** (2007), 1883.
24) T. P. Fredman, J. Torrkulla and H. Saxen: *Metall. Mater. Trans. B*, **30** (1999), 323.